InletTracker: An open-source Python toolkit for historic and near real-time monitoring of coastal inlets from Landsat and Sentinel-2

Valentin Heimhuber, Kilian Vos, Wanru Fu, William Glamore

Supplementary material

S1. Accuracy metrics used to assess the performance for predicting binary inlet states

After classifying the Δ-to-median series into binary open vs. closed inlet states, we first computed true positives (TP), false positives (FP), true negatives (TN) and false negatives (FN). We then calculated Accuracy as the fraction of all correct classifications over all samples in line with Equation 1 (Kotu and Deshpande, 2015). Open inlet states are considered 'positives' in these calculations.

$Accuracy = (TP+TN)/(TP+FP+FN+TN)$ (Eq. 1)

The F1 score is essentially a weighted average of precision and recall, where the precision is the proportion of correct positive cases to the tested positive cases. It reflects how precise the prediction is (Kotu and Deshpande, 2015).

$Precision = TP/(TP+FP)$ (Eq. 2)

In comparison, recall is the proportion of correct positive cases to real positive cases. It represents how well the system captures the targeted cases (Kotu and Deshpande, 2015).

$Recall = TP/(TP+FN)$ (Eq. 3)

The F1 score combines precision and recall together in the form of a harmonic mean that ranges between 0 and 1 (Kotu and Deshpande, 2015).

$F1 = 2 \times (Precision \times Recall)/(Precision + Recall)$ (Eq. 4)

S2. Accuracy assessment results for high resolution monitoring of inlet dynamics via Sentinel-2 only (2016-2020)

Table S1: Validation statistics obtained via comparison of algorithm results against visually inferred inlet states for the S2 record only. Statistics are provided separately for the across-berm (A-B) and along-berm (C-D) transects. The number of images available for each site and number of open vs. closed visually inferred inlet states is also provided. The optimal classification threshold was used to classify images into open vs. closed states based on the Δ-to-median parameter, where Δ-to-median > threshold = open.

Inlet site	Transect direction	F1-score	Accu-racy	True neg.	False pos.	False neg.	True pos.	Optimal classific. Threshold	Total nr. Of images	Nr. Of closed images	Nr. Of open images
Inmanriver	A-B	0.71	0.79	65	11	14	31	0.01	121	76	45
	C-D	0.70	0.80	69	7	17	28	0.08	-	-	-
Curl Curl	A-B	0.65	0.90	149	9	9	17	0.01	184	158	26
	C-D	0.63	0.90	149	9	10	16	0.04	-	-	-
Dee Why	A-B	0.69	0.90	159	0	21	23	0.02	203	159	44
	C-D	0.66	0.87	150	9	18	26	0.03	-	-	-
Coila	A-B	1.00	1.00	119	0	0	6	0.01	125	119	6
	C-D	1.00	1.00	119	0	0	6	0.03	-	-	-
Wamberal	A-B	0.89	0.98	199	2	3	20	0.03	224	201	23
	C-D	0.91	0.98	199	2	2	21	0.04	-	-	-
Narrabean	A-B	0.98	0.98	59	3	0	65	0.09	127	62	65
	C-D	0.97	0.97	58	4	0	65	0.06	-	-	-
Nadgee	A-B	0.75	0.99	170	0	2	3	0.03	175	170	5
	C-D	0.33	0.95	165	5	3	2	0.15	-	-	-
Hamersley Inlet	A-B	1.00	1.00	96	0	0	1	0.02	97	96	1
	C-D	1.00	1.00	96	0	0	1	0.05	-	-	-
Conjola	A-B	0.94	0.95	48	1	4	42	0.01	95	49	46
	C-D	0.94	0.95	48	1	4	42	0.04	-	-	-
Durras	A-B	0.98	0.98	57	1	2	72	0.02	132	58	74
	C-D	0.99	0.98	58	0	2	72	0.09	-	-	-
Stokes Inlet	A-B	0.00	0.94	129	7	1	0	0.01	137	136	1
	C-D	0.00	0.58	80	56	1	0	0.01	-	-	-
Irwin Inlet	A-B	0.91	0.93	38	1	4	26	0.02	69	39	30
	C-D	0.92	0.93	36	3	2	28	0.02	-	-	-
Average	A-B	0.75	0.91	-	-	-	-	0.05	141	110	31
Average	C-D	0.79	0.94	-	-	-	-	0.02	-	-	-

S3. Recommendations for optimal band and index selection

To account for the unique spectral characteristics of different coastal inlets, InletTracker currently provides NIR, SWIR1, NDWI and mNDWI as options for path finding and inferring of open vs. closed inlet states. These options are in line with the majority of state-of-the-art coastal shoreline or waterline mapping methods that either use a single band NIR or SWIR1/2 approach (Cabezas-Rabadán et al., 2020; Pardo-pascual et al., 2018; Ryu et al., 2002), or an approach based on a spectral index involving the green, NIR and/or SWIR bands (Bishop-taylor et al., 2019; Son et al., 2020; Vos et al., 2019). The performance of each of the four band/index options could not be explicitly tested as part of this work due to a lack of suitable in-situ validation data such as GPS transects. To provide recommendations in the absence of such data, a brief review of the relevant physical characteristics of the four options is provided here followed by a targeted analysis of six unique along-berm transects.

The reduced reflectance in the visible, NIR and SWIR wavelengths over water is the result of absorption and scattering of the electromagnetic radiation as it traverses the water column (Green et al., 2000). For pure water, the absorption of radiation increases exponentially from visible to NIR wavelengths and beyond (Green et al., 2000; Pope and Fry, 1997). For wavelengths above 1µm, such as those measured by the SWIR1 band, absorption is very high, even for turbid water (Liu et al., 2019). As a consequence, scattered puddles or wet mud that may be present in tidal flats can cause sufficient absorption in the SWIR range for exposed mudflats to be misclassified as standing water (Ryu et al., 2008). In the NIR band, on the other hand, there is a risk of shallow water areas being falsely classified as 'dry', due to lower absorption levels in water (compared to the SWIR range) and increased reflectance due to scattering in the presence of high suspended sediment content (Liu et al., 2019; Lodhi et al., 1997) and/or phytoplankton (Gitelson, 1992). Lastly, the NIR band is significantly affected by white water in the surf zone (Pardo-pascual et al., 2018; Ryu et al., 2002), which typically leads to elevated NIR reflectance (see across-berm paths avoiding white water in Figure 5) and the NDWI shifting towards the 'dry' range. Indices such as NDWI and mNDWI take advantage of the fact that attenuation in the green range is much lower than in the NIR or SWIR ranges consistently for a wide range of different surface water features (Fisher et al., 2016; Mcfeeters, 1996; Xu, 2007). Both indices use the green band as part of a normalized difference ratio, so that their different behaviour largely corresponds to the aforementioned characteristics of the NIR and SWIR bands.

Many of the unique band and index features discussed above can be readily observed by analyzing NIR, SWIR1, NDWI and mNDWI transects over a common along-berm or across-berm path shown in Figure 9 for six example S2 images (three images during closed and three images during open inlet states). The higher sensitivity of the SWIR1 compared to the NIR band is illustrated well in the wider and deeper depressions over open inlets obtained for SWIR1. This is especially evident on the image of the 20-08-2020, where both the SWIR1 and the mNDWI$^{(-1)}$ indicate lower (in comparison to dry sand) values of around 0 for the tip of the southern berm adjacent to the channel (see solid blue lines). While this feature is, albeit less pronounced, also captured by the NIR band, it is lost in the NDWI. Unfortunately, it remains unclear whether the tip of the southern berm was covered with water or just wet sand in this example. Considering the tide level of 0.52m above mean sea level (AMSL) at the time of image capture (not shown), it is possible that shallow inundation was present around the transect in this section. The transects also illustrate that the normalized difference indices effectively eliminate the variability in reflectance that is present in both the SWIR1 and NIR bands over the dry berm areas along the path (see uneven and variable SWIR1 and NIR transects during closed inlets). In these dry berm areas, the NDWI and mNDWI indices exhibit stable values of around 0.2 and 0.3, respectively. Although these mean values can fluctuate from image to image due to lighting conditions and other factors (e.g., Figure 6e), this narrow spectral range is what enables our method to consistently infer the reflectance of dry berm areas via the median of the along-berm transect.

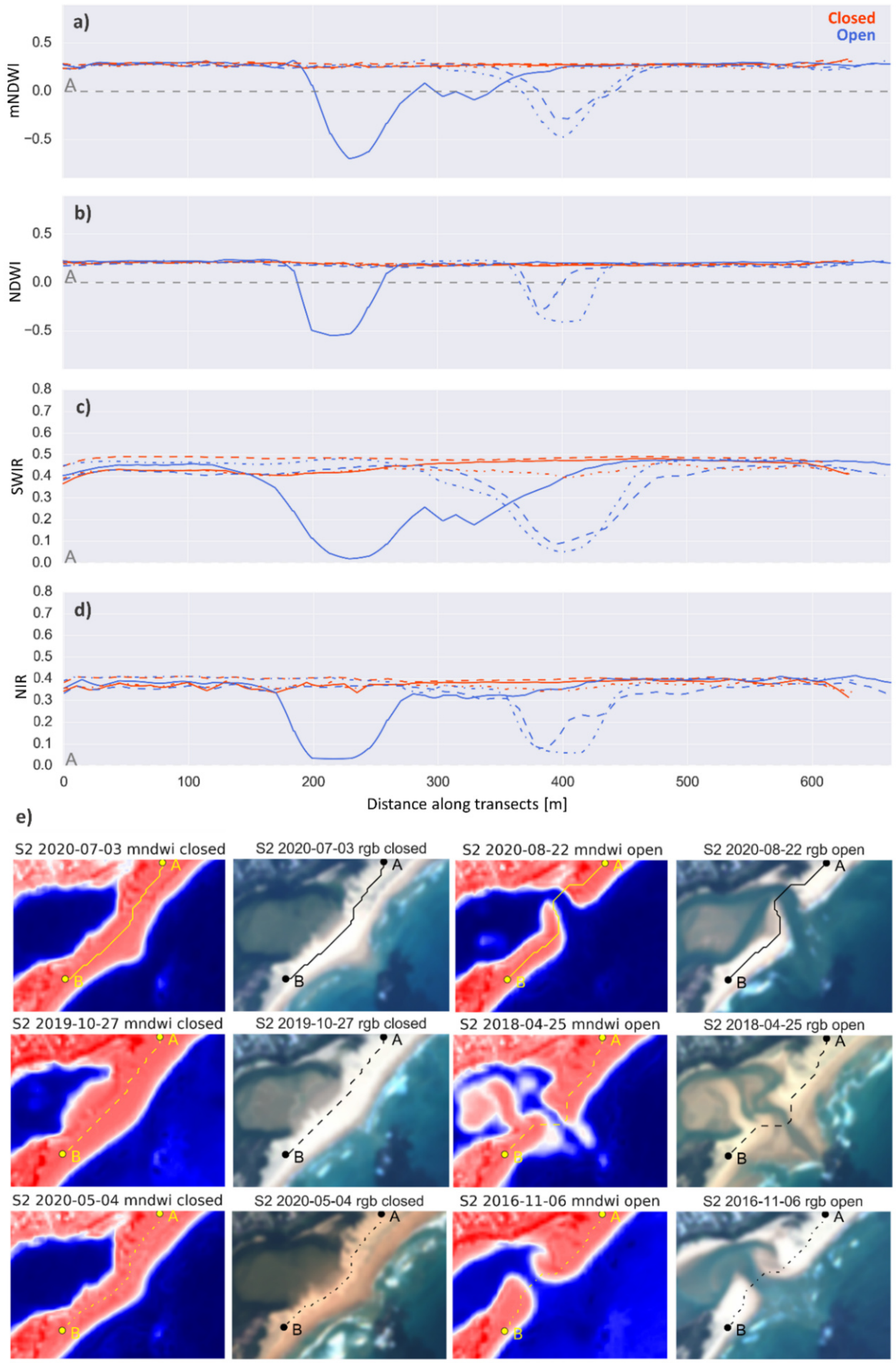

85

86 **Figure S1:** Comparison of NIR, SWIR1, NDWI and mNDWI for analysing inlet states based on three

87 S2 images during open (blue lines) and three S2 images during closed inlet states (red lines).

88

Based on the physical characteristics discussed above and the experiments presented in this paper, we provide the following recommendations for inlet state detection via InletTracker.

- For pathfinding, it is advantageous to use either the NIR or SWIR1 band directly and use a mask to exclude heavily confounding classes such as vegetation or built-up areas.
- For inferring inlet states, on the other hand, it is recommended to use the normalized difference ratios as these provide a robust approximation of dry sand reflectance via the median of the along-berm transect.
- It is recommended to use the single band that corresponds to the index that is subsequently used for inferring inlet states (i.e., NIR/NDWI or SWIR1/mNDWI).
- The SWIR1/mNDWI approach provides a higher sensitivity for detecting very shallow or narrow inlet openings. Conversely, this high sensitivity to shallow waters and wet sand or mud can sometimes lead to falsely classifying a closed inlet as open.
- The NIR/NDWI approach is generally more conservative due to the lower sensitivity of the NIR band for very shallow waters. The low sensitivity to shallow waters can lead to classifying open inlet states as closed, especially when the image was acquired during low tide.
- For S2, the NIR band is of 10m resolution compared to 15m resolution of the SWIR1 band and as such, the S2 NIR/NDWI configuration is advantageous for IOCEs with small inlet channels.
- In the presence of highly turbid waters or large amounts of white water in or near the inlet channel, the SWIR1/mNDWI approach is likely to be more robust than the NIR/NDWI approach, due to the limited sensitivity of the SWIR1 band to these features.

In practice, we further recommend doing test runs for path finding using different seed and receiver point locations as well as band and index combinations. This will ensure that the optimal algorithm configuration is established before processing the full imagery archive.

References

Bishop-taylor, R., Sagar, S., Lymburner, L., Alam, I., Sixsmith, J., 2019. Sub-Pixel Waterline Extraction : Characterising Accuracy and Sensitivity to Indices and Spectra. Remote Sens. 2019, 11, 2984. https://doi.org/10.3390/rs11242984

Cabezas-Rabadán, C., Pardo-Pascual, J.E., Palomar-Vázquez, J.M., Fernández-Sarría, A., 2020. An efficient protocol for accurate and massive shoreline definition from mid-resolution satellite imagery. Coast. Eng. 160. https://doi.org/10.1016/j.coastaleng.2020.103732

Fisher, A., Flood, N., Danaher, T., 2016. Comparing Landsat water index methods for automated water classification in eastern Australia. Remote Sens. Environ. 175, 167–182. https://doi.org/10.1016/j.rse.2015.12.055

Gitelson, A., 1992. The peak near 700 nm on radiance spectra of algae and water: relationships of its magnitude and position with chlorophyll concentration. Int. J. Remote Sens. 13. https://doi.org/10.1080/01431169208904125

Green, E.P., Mumby, P.J., Edwards, A.J., Clark, C.D., 2000. Remote Sensing Handbook for Tropical Coastal Management, Remote Sensing Handbook for Tropical Coastal Management. https://doi.org/10.1109/6.367967

Kotu, V., Deshpande, B., 2015. Model Evaluation, in: Predictive Analytics and Data Mining. https://doi.org/doi: 10.1016/b978-0-12-801460-8.00008-2.

Liu, H., Hu, S., Zhou, Q., Li, Q., Wu, G., 2019. Revisiting effectiveness of turbidity index for the switching scheme of NIR- SWIR combined ocean color atmospheric correction algorithm. Int J Appl Earth Obs Geoinf. 76, 1–9. https://doi.org/10.1016/j.jag.2018.10.010

Lodhi, M.A., Rundquist, D.C., Han, L., Kuzila, M.S., 1997. The potential for remote sensing of loewss soils suspended in surface waters. J. Am. WATER Resour. Assoc. 33.

Mcfeeters, S.K., 1996. The use of the Normalized Difference Water Index (NDWI) in the delineation of open water features. Int. J. Remote Sens. 17, 1425–1432. https://doi.org/10.1080/01431169608948714

Pardo-pascual, J.E., Elena, S., Almonacid-caballer, J., 2018. Assessing the Accuracy of Automatically Extracted Shorelines on Microtidal Beaches from Landsat 7 , Landsat 8 and Sentinel-2 Imagery. Remote Sens. 10.

https://doi.org/10.3390/rs10020326

Pope, R.M., Fry, E.S., 1997. Absorption spectrum (380–700 nm) of pure water. II. Integrating cavity measurements. Appl. Opt. 36.

Ryu, J., Kim, C., Lee, Y., Won, J., Chun, S., Lee, S., 2008. Detecting the intertidal morphologic change using satellite data. Estuar. Coast. Shelf Sci. 78, 623–632. https://doi.org/10.1016/j.ecss.2008.01.020

Ryu, J., Won, J., Min, K.D., 2002. Waterline extraction from Landsat TM data in a tidal flat A case study in Gomso Bay , Korea 83, 442–456. https://doi.org/10.1016/S0034-4257(02)00059-7

Son, S., Paul, J., Lan, T., 2020. An optimal waterline approach for studying tidal flat morphological changes using remote sensing data: A case of the northern coast of Vietnam. Estuar. Coast. Shelf Sci. 236, 106613. https://doi.org/10.1016/j.ecss.2020.106613

Vos, K., Harley, M.D., Splinter, K.D., Simmons, J.A., Turner, I.L., 2019. Sub-annual to multi-decadal shoreline variability from publicly available satellite imagery. Coast. Eng. 150, 160–174. https://doi.org/10.1016/j.coastaleng.2019.04.004

Xu, H., 2007. Modification of normalised difference water index (NDWI) to enhance open water features in remotely sensed imagery 1161. https://doi.org/10.1080/01431160600589179